Syntheses, structures, spectroscopic and electrochemical properties of two 1D organic–inorganic Cu^{II}–Ln^{III} heterometallic germanotungstates

Jingli Zhang [a], Jie Li [a], Lijie Li [a], Haozhe Zhao [a], Pengtao Ma [a], Junwei Zhao [a,b,*], Lijuan Chen [a,c,*]

[a] Institute of Molecular and Crystal Engineering, Henan Key Laboratory of Polyoxometalate Chemistry, College of Chemistry and Chemical Engineering, Henan University, Kaifeng, Henan 475004, PR China
[b] State Key Laboratory of Structural Chemistry, Fujian Institute of Research on the Structure of Matter, Chinese Academy of Sciences, Fuzhou, Fujian 350002, PR China
[c] Basic Experiment Teaching Center, Henan University, Kaifeng, Henan 475004, PR China

HIGHLIGHTS

- Copper–lanthanide heterometallic germanotungstate.
- IR spectra of copper–lanthanide heterometallic germanotungstates.
- Photoluminescence spectra of germanotungstates.
- The electrocatalytic activity for nitrite reduction.

GRAPHICAL ABSTRACT
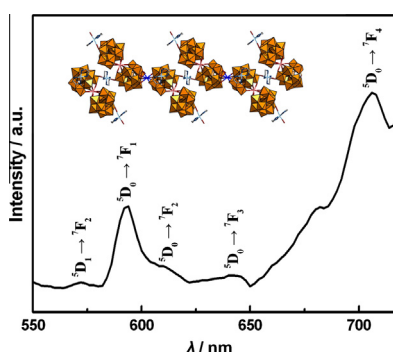
ABSTRACT

Two organic–inorganic hybrid copper–lanthanide heterometallic germanotungstates KNa$_2$H$_7$[enH$_2$]$_3$ [Cu(en)$_2$(H$_2$O)]$_2$[Cu(en)$_2$]$_2${Cu(en)$_2$[Eu(α-GeW$_{11}$O$_{39}$)$_2$]$_2$}·13H$_2$O (**1**) and Na$_2$H$_4$[Cu(en)$_2$(H$_2$O)]$_2$[Cu(en)$_2$]$_6$ [Cu(en)$_2$]{Cu(en)$_2$[La(α-GeW$_{11}$O$_{39}$)$_2$]$_2$}·12H$_2$O (**2**) have been hydrothermally synthesized by reaction of K$_8$Na$_2$[A-α-GeW$_9$O$_{34}$]·25H$_2$O with CuCl$_2$·2H$_2$O and EuCl$_3$/LaCl$_3$ in the presence of en (en = ethylenediamine) and structurally characterized by elemental analyses, IR spectra and single-crystal X-ray diffraction. **1** exhibits the 1D chain motif built by tetrameric {[Cu(en)$_2$(H$_2$O)]$_2$[Cu(en)$_2$]$_2${Cu(en)$_2$[Eu(α-Ge W$_{11}$O$_{39}$)$_2$]$_2$}}$^{16-}$ moieties through square antiprismatic K$^+$ cations while **2** displays the 1D architecture made by tetrameric [[Cu(en)$_2$]$_6$[Cu(en)$_2$]{Cu(en)$_2$[La(α-GeW$_{11}$O$_{39}$)$_2$]$_2$}]$^{10-}$ units via octahedral [Cu(en)$_2$]$^{2+}$ cations. Furthermore, the solid-state electrochemical and electrocatalytic properties of **1** have been investigated and **1** indicates the good electrocatalytic activity for nitrite reduction. In addition, the photoluminescence property of **1** has been investigated.

© 2013 Elsevier B.V. All rights reserved.

Introduction

Polyoxometalates (POMs) have attracted increasing interest not only because they can act as anionic metal–oxygen clusters to afford versatile inorganic nucleophilic polydentate building blocks for transition-metal (TM) or lanthanide (Ln) cations but also their potential applications in catalysis, magnetism, electrochemistry and materials science [1–7]. In recent years, germanotungstates (GTs) as an important subfamily of POM chemistry have gradually become a new research focus and a challengeable area. Numerous fresh TM substituted GTs have been consecutively obtained such as [Mn$_4$^{III}(H$_2$O)$_2$(GeW$_9$O$_{34}$)$_2$]$^{8-}$ [8], [Cu$_3$(H$_2$O)(B-β-GeW$_9$O$_{33}$(OH)) (B-β-GeW$_8$O$_{30}$(OH))]$^{12-}$ [9], [Co(H$_2$O)$_2${Co$_3$(B-β-GeW$_9$O$_{33}$(OH)) (B-β-GeW$_8$O$_{30}$(OH))}$_2$]$^{22-}$ [9], [Mn(H$_2$O)$_2${Mn$_3$(H$_2$O)(B-β-GeW$_9$

* Corresponding authors at: Institute of Molecular and Crystal Engineering, Henan Key Laboratory of Polyoxometalate Chemistry, College of Chemistry and Chemical Engineering, Henan University, Kaifeng, Henan 475004, PR China. Tel./fax: +86 378 3886876.
E-mail addresses: zhaojunwei@henu.edu.cn (J. Zhao), ljchen@henu.edu.cn (L. Chen).

$O_{33}OH))(B-\beta-GeW_8O_{30}(OH))_2]^{22-}$ [9], $[Zr_3O(OH)_2(\alpha-GeW_9O_{34})$ $(\beta-GeW_9O_{34})]^{12-}$ [10], $[M_4(H_2O)_2(GeW_9O_{34})_2]^{12-}$ ($M = Mn^{II}$, Zn^{II}, and Cd^{II}) [11], $[n-BuNH_3]_{12}[Cu_4(GeW_9O_{34})_2]\cdot14H_2O$ [12], $[Fe_6$ $(OH)_3(A-\alpha-GeW_9O_{34}(OH)_3)_2]^{11-}$ [13], $[K(H_2O)(\beta-Fe_2GeW_{10}O_{37}$ $(OH))(\gamma-GeW_{10}O_{36})]^{12-}$ [14], $[\{\beta-Fe_2GeW_{10}O_{37}(OH)_2\}_2]^{12-}$ [14], $[Mn_6Ge_3W_{24}O_{94}(H_2O)_2]^{18-}$ [15], $[Cu(H_2O)_2]H_2[Cu_8(dap)_4(H_2O)_2$ $(\alpha-B-GeW_9O_{34})_2]$ [16] and $[Cu(deta)(H_2O)_2]_2[Cu_6(en)_2(H_2O)_2$ $(B-\alpha-GeW_9O_{34})_2]\cdot6H_2O$ [17]. On the other hand, Ln^{III} ions, by means of their multiple coordination numbers and strong oxophilicity, can be used as effective and multifunctional linkers in the preparations of Ln-containing GTs, and some typical examples are as follows: $[\{Ln_2\}(\alpha(1,4)-GeW_{10}O_{38})(H_2O)_3\}_2]^{12-}$ ($Ln = Dy^{III}$ or Er^{III}) [18], $[Ce_{20}Ge_{10}W_{100}O_{376}(OH)_4(H_2O)_{30}]^{56-}$ [19], $[Dy(H_2O)_4]_{0.25}[Dy$ $(H_2O)_6]_{0.25}H_{0.5}\{Dy(H_2O)_7[Dy(H_2O)_2(DMSO)(\alpha-GeW_{11}O_{39})]\}\cdot5.25H_2O$ [20], $[(CH_3)_4N]_2H_{1.50}[Nd_{1.50}(GeW_{11}O_{39})(H_2O)_6]\cdot3H_2O$ [21], $[(CH_3)_4-$ $N]_2H_{2.25}[Sm_{1.25}(GeW_{11}O_{39})(H_2O)_4]\cdot3.75H_2O$ [21], $[(CH_3)_4N]_{2.50-}$ $H_{2.50}[Y(GeW_{11}O_{39})(H_2O)_2]\cdot4H_2O$ [21], $[(CH_3)_4N]_{2.50}H_{2.50}Yb(GeW_{11}$ $O_{39})$ $(H_2O)_2]\cdot3.75H_2O$ [21] and $[K{\subset}K_7Ce_{24}Ge_{12}W_{120}O_{456}$ $(OH)_{12}$ $(H_2O)_{64}]^{52-}$ [1]. In contrast, little work has been dedicated to the study of TM–Ln heterometallic GTs. To the best of our knowledge, only a few examples have been reported. For example, in 2009, Reinoso's group reported a rhomblike-$Ce^{III}_2Mn^{III}_2O_{20}$ substituted GT $[\{Ce(H_2O)_2\}_2Mn_2(B-\alpha-GeW_9O_{34})_2]^{8-}$ [22], later, they communicated a new type of Cu^{II}–Ce^{IV} heterometallic GT hybrid $[\{Ce^{IV}$ $(OAc)\}Cu^{II}_3(H_2O)(B-\alpha-GeW_9O_{34})_2]^{11-}$ [23]. In 2011, Yang et al. addressed a novel Keggin-type GT containing heterometallic Cu–Dy cubane clusters $\{[Cu(en)_2(H_2O)][DyCu_3(en)_3(OH)_3(H_2O)_2(GeW_{11-}$ $O_{39})]\}_2\cdot18H_2O$ [24]. As a result, the design and preparation of TM–Ln heterometallic GTs is still a challenging task. Recently, our attention has been paid on this field on the basis of the following four ideas: (1) In comparison with other TM caions, Cu^{II} ions have more flexible various coordination configurations (square, trigonal bipyramid, square pyramid and octahedron); (2) Ln cations, with their high and variable coordination numbers and flexible coordination geometry, provide good opportunities for discovering of complicated structures; (3) Combination of the flexible coordination requirements of Cu^{II} ions and strong oxophilicity of Ln cations with the labile lacunary GT precursors can construct novel Cu–Ln heterometallic GT derivatives; (4) The presence of the Jahn–Teller effect of the octahedral and pseudo-Jahn–Teller effect of the square pyramids for Cu^{II} cations may overcome larger steric hindrance and contribute to stabilize the in situ formed GT derivatives [25,26], thus, a family of organic–inorganic hybrid GT-based Cu–Ln heterometallic derivatives $\{[Cu(en)_2(H_2O)][Cu_3Tb(en)_3$ $(OH)_3$ $(H_2O)_2](\alpha-GeW_{11}O_{39})\}_2\cdot11H_2O$, $\{[Cu(en)_2(H_2O)][Cu_3Dy(en)_3$ $(OH)_3$ $(H_2O)_2](\alpha-GeW_{11}O_{39})\}_2\cdot10H_2O$, $K_4H_2[Cu(en)_2(H_2O)_2]_5[Cu$ $(en)_2$ $(H_2O)]_2[Cu(en)_2]_2\{Cu(en)_2[Pr(\alpha-GeW_{11}O_{39})_2]_2\}\cdot16H_2O$ and KNa_3H_6 $[enH_2]_3[Cu(en)_2(H_2O)]_2[Cu(en)_2]_2\{Cu(en)_2[Er(\alpha-GeW_{11-}$ $O_{39})_2]_2\}\cdot12$ H_2O have been firstly isolated [26]. As a part of our ongoing research, two new organic–inorganic hybrid Cu–Ln heterometallic GTs $KNa_2H_7[enH_2]_3[Cu(en)_2$ $(H_2O)]_2[Cu(en)_2]_2$ $\{Cu(en)_2$ $[Eu(\alpha-GeW_{11}O_{39})_2]_2\}\cdot13H_2O$ (1) and $Na_2H_4[Cu(en)_2(H_2O)]_2$ $[Cu$ $(en)_2]_6\{Cu(en)_2[La(\alpha-GeW_{11}O_{39})_2]_2\}\cdot12H_2O$ (2) have been consecutively isolated and characterized by elemental analyses, IR spectra and single-crystal X-ray diffraction. Structural analyses show that 1 exhibits the 1D chain motif constructed from tetrameric $\{[Cu(en)_2(H_2O)]_2[Cu(en)_2]_2\{Cu(en)_2[Eu(\alpha-GeW_{11}$ $O_{39})_2]_2\}\}^{16-}$ moieties through square antiprismatic K^+ cations whereas 2 utilizes the 1D chain fashion formed by tetrameric $[[Cu(en)_2]_6[Cu(en)_2]$ $\{Cu(en)_2[La(\alpha-GeW_{11}O_{39})_2]_2\}]^{10-}$ units via octahedral $[Cu(en)_2]^{2+}$ cations. The solid-state electrochemical and electrocatalytic properties of 1 have been carried out in 0.5 mol L^{-1} $Na_2SO_4 + H_2SO_4$ aqueous solution (pH = 0.8) by entrapping it in a carbon paste electrode owing to 1 prepared by hydrothermal reaction being of insolubility in water. In addition, the photoluminescence property of 1

has been investigated and 1 displays the characteristic emissions of the Eu^{3+} ions.

Experimental

Materials and physical measurements

$K_8Na_2[A-\alpha-GeW_9O_{34}]\cdot25H_2O$ was synthesized according to Ref. [13]. All other reagents were of analytical grade and used as purchased without further purification. Elemental analyses (C, H and N) were performed on a Perkin–Elmer 240 °C elemental analyzer. Inductively coupled plasma atomic emission spectra were performed on a Perkin–Elmer Optima 2000 ICP–AES spectrometer. IR spectra were obtained from a sample powder palletized with KBr on a Nicolet 170 SXFT-IR spectrophotometer over the range of 4000–400 cm^{-1}. Cyclic voltammograms were recorded on a CS electrochemical workstation (Wuhan CorrTest Instrument Co. Ltd.) at room temperature. A conventional three-electrode system was used. Platinum gauze was used as a counter electrode and an Ag/AgCl electrode was referenced. Chemically bulk-modified carbon paste electrode (CPEs) was used as the working electrode. A PHB-4 type pH meter was used for pH measurement. The emission spectrum was recorded on a HITACHI F-7000 fluorescence spectrophotometer.

Synthesis of 1

A mixture of $K_8Na_2[A-\alpha-GeW_9O_{34}]\cdot25H_2O$ (0.307 g, 0.100 mmol), $CuCl_2\cdot2H_2O$ (0.098 g, 0.575 mmol), $EuCl_3$ (0.202 g, 0.781 mmol), en (0.10 mL, 1.494 mmol) and H_2O (5 mL, 278 mmol) was stirred for 2 h, sealed in a 25 mL Teflon-lined steel autoclave, kept at 160 °C for 5 days and then cooled to room temperature. Purple prismatic crystals were obtained by filtering, washed with distilled water and dried in air at ambient temperature. Yield: ca. 21% (based on $K_8Na_2[A-\alpha-GeW_9O_{34}]\cdot25H_2O$). Anal. calcd. (found %) for $C_{26}H_{147}Cu_5Eu_2Ge_4KN_{26}Na_2O_{171}W_{44}$ (1): C 2.47 (2.60), H 1.17 (1.33), N 2.88 (2.72), Na 0.36 (0.45), K 0.31 (0.25), Cu 2.51 (2.64), Ge 2.30 (2.39), W 63.96 (63.88), and Eu 2.40 (2.47).

Synthesis of 2

The synthetic procedure of 2 was identical to 1 with a mixture of $K_8Na_2[A-\alpha-GeW_9O_{34}]\cdot25H_2O$ (0.608 g, 0.198 mmol), $CuCl_2\cdot2H_2O$ (0.104 g, 0.610 mmol), $LaCl_3$ (0.098 g, 0.399 mmol), en (0.10 mL, 1.494 mmol) and H_2O (5 mL, 278 mmol). Purple prismatic crystals were also obtained. Yield: ca. 23% (based on $K_8Na_2[A-\alpha-GeW_9O_{34}]$ $\cdot25H_2O$). Anal. calcd. (found %) for $C_{40}H_{192}Cu_{10}Ge_4La_2N_{40}Na_2O_{170-}$ W_{44} (2): C 3.61 (3.80), H 1.46 (1.62), N 4.21 (4.07), Na 0.35 (0.47), Cu 4.78 (4.66), Ge 2.18 (2.28), W 60.85 (60.69), and La 2.09 (2.20).

Preparation of 1-CPE

1-CPE was fabricated as follows: 30 mg of graphite powder and 10 mg of 1 were mixed and ground together by an agate mortar and pestled to form an uniform mixture, and then 0.05 mL of Nujol was added with stirring. The homogenized mixture was packed into a glass tube with a 3.0 mm inner diameter, and the tube surface was wiped with paper. Electrical contact was established with a Cu rod through the back of the electrode.

X-ray crystallographic determination

A single crystal of 1 or 2 suitable for X-ray crystallography was carefully selected under an optical microscope and glued to a thin glass fiber. Diffraction data for 1 and 2 were collected on a Bruker

APEX-II CCD diffractometer using graphite monochromatized Mo Kα radiation (λ = 0.71073 Å) at 296(2) K. Intensity data were collected using the ω scan technique. Routine Lorentz polarization and empirical absorption corrections were applied. Their structures were solved by direct methods and refined using full-matrix least-squares on F^2. All calculations were performed using the SHELXTL-97 program package [27,28]. No hydrogen atoms associated with water molecules were located from the difference Fourier map. Positions of the hydrogen atoms attached to carbon and nitrogen atoms were geometrically placed. All hydrogen atoms were refined isotropically as a riding mode using the default SHELXTL parameters. All non-hydrogen atoms were refined anisotropically except for some carbon atoms and water molecules. Crystal data and structure refinements for **1–2** are listed in Table 1.

Results and discussion

Synthesis

Trivacant Keggin GT $[A-\alpha-GeW_9O_{34}]^{10-}$ precursor can act as a polydentate ligand for TM or Ln cations forming TM or Ln substituted GTs with diverse metal nuclearities and beautiful structures under either conventional aqueous solution or hydrothermal environments [8,13,16,17,22,23]. The $K_8Na_2[A-\alpha-GeW_9O_{34}]\cdot25H_2O$ precursor was firstly introduced to hydrothermal reactions by us in 2008 [16,29]. When it was reacted with $CuCl_2\cdot2H_2O$ in the present of en or dap (1,2-diaminopropane) or 2,2′-bpy (2,2′-bipyridine) at 100 or 150 °C, a class of novel organic–inorganic hybrid octa-Cu sandwiched GTs $(H_2en)_2[Cu_8(en)_4(H_2O)_2(B-\alpha-GeW_9O_{34})_2]\cdot5H_2O$ (Fig. 1a) [29], $[Cu(H_2O)_2]H_2[Cu_8(dap)_4(H_2O)_2(\alpha-B-GeW_9O_{34})_2]$ (Fig. 1b) [16] and $[Cu^{II}_2(H_2O)_2(2,2′-bpy)_2]\{[Cu^{II}(bdyl)]_2[Cu^{II}_8(2,2′-bpy)_4(H_2O)_2(B-\alpha-GeW_9O_{34})_2]\}\cdot4H_2O$ (Fig. 1c) [29]. Similarly, when it was reacted with $NiCl_2\cdot6H_2O$ in the present of en or dap at 100 °C, two ferromagnetic hexa-Ni substituted GT hybrids $[Ni(en)_2]_{0.5}[\{Ni_6(\mu_3-OH)_3(en)_3(H_2O)_6\}(B-\alpha-GeW_9O_{34})]\cdot3H_2O$ (Fig. 1d) and $[\{Ni_6(\mu_3-OH)_3(dap)_3(H_2O)_6\}(B-\alpha-GeW_9O_{34})]\cdot H_3O\cdot4H_2O$ were synthesized [30]. Subsequently, the reactivity of it with $CuCl_2\cdot2H_2O$ in the participation of deta (diethylenetriamine) at 130 °C led to the $6^5\cdot8$ CdSO₄-type 3-D framework built by hexa-Cu^{II} sandwiched polyoxotungstates $[Cu(en)_2]_2[Cu(deta)(H_2O)]_2[Cu_6(en)_2(H_2O)_2(B-\alpha-GeW_9O_{34})_2]\cdot6H_2O$ (Fig. 1f) with mixed organic ligands [17]. Furthermore, $K_8Na_2[A-\alpha-GeW_9O_{34}]\cdot25H_2O$, $NiSO_4\cdot7H_2O$ and en were utilized at 160 °C affording a hexa-Ni^{II} sandwiched GT

$[enH_2]_2[Ni(en)_2]_2\{[Ni_6(en)_2(H_2O)_2][B-\alpha-GeW_9O_{34}]_2\}\cdot14H_2O$ (Fig. 1e) [31]. Recently, with the design and preparation of TM–Ln heterometallic polyoxotungstates becoming an emerging focus in POM chemistry, the reaction system containing $K_8Na_2[A-\alpha-GeW_9O_{34}]\cdot25H_2O$ with TM and Ln mixed cations in the presence of organic components was explored by our lab. The mixture of $K_8Na_2[A-\alpha-GeW_9O_{34}]\cdot25H_2O$, $CoCl_2\cdot6H_2O$, $PrCl_3$ and dap was firstly employed at 160 °C, unexpectedly, a 2-D organic–inorganic hybrid tetra-Co^{II}-substituted sandwich-type GT $\{[Co(dap)_2(H_2O)]_2[Co(dap)_2]_2[Co_4(Hdap)_2(B-\alpha-HGeW_9O_{34})_2]\}\cdot7H_2O$ (Fig. 1g) was isolated [32]. Although $PrCl_3$ was used in the reaction, no Pr^{III} ion was observed in the product. The paralleling experiments indicated that only amorphous powder was obtained when removing $PrCl_3$ away from the reaction. $PrCl_3$ may play a synergistic action with other components in the reaction. With the deepening of research in this field, when the reaction was performed with $K_8Na_2[A-\alpha-GeW_9O_{34}]\cdot25H_2O/CuCl_2\cdot2H_2O/EuCl_3$ in the presence of en at 160 °C, a unique $\{Cu_3EuO_4\}$ cubane substituted GT $\{[Cu(en)_2(H_2O)][Cu_3Eu(en)_3(OH)_3(H_2O)_2](\alpha-GeW_{11}O_{39})\}_2\cdot11H_2O$ was discovered (Fig. 1h) [26]. When $TbCl_3$ and $DyCl_3$ replaced $EuCl_3$, the analogues $\{[Cu(en)_2(H_2O)][Cu_3Tb(en)_3(OH)_3(H_2O)_2](\alpha-GeW_{11}O_{39})\}_2\cdot11H_2O$ and $\{[Cu(en)_2(H_2O)][Cu_3Dy(en)_3(OH)_3(H_2O)_2](\alpha-GeW_{11}O_{39})\}_2\cdot10H_2O$ were obtained [26]. However, $LaCl_3/PrCl_3/ErCl_3$ were used under similar reaction conditions, we prepared three POM hybrids built by Ln-containing GTs and copper-en complexes $Na_2H_6[Cu(en)_2(H_2O)]_8\{Cu(en)_2[La(\alpha-GeW_{11}O_{39})_2]_2\}\cdot18H_2O$, $K_4H_6[Cu(en)_2(H_2O)]_5[Cu(en)_2(H_2O)]_2[Cu(en)_2]_2\{Cu(en)_2[Pr(\alpha-GeW_{11}O_{39})_2]_2\}\cdot16H_2O$ (Fig. 1i) and $KNa_2H_7[enH_2]_3[Cu(en)_2(H_2O)]_2[Cu(en)_2]_2\{Cu(en)_2[Er(\alpha-GeW_{11}O_{39})_2]_2\}\cdot15H_2O$, which are completely distinct from those $\{Cu_3LnO_4\}$ cubane substituted GTs [26]. With our systematic exploration, another two organic–inorganic Cu–Ln heterometallic GTs **1** (Fig. 1j) and **2** (Fig. 1k) have been hydrothermally synthesized. The above-mentioned results suggest that the molar ratios of $K_8Na_2[A-\alpha-GeW_9O_{34}]\cdot25H_2O/CuCl_2\cdot2H_2O/LnCl_3$ have an important influence on the structural diversity of the resulting GT derivatives. Other else, the common structural features of **1**, **2**, $\{Cu_3EuO_4\}$ cubane substituted GTs and three POM hybrids built by Ln-containing GTs and copper-en complexes are that all contain monovacant $[\alpha-GeW_{11}O_{39}]^{8-}$ fragments, however, when $K_6Na_2[\alpha-GeW_{11}O_{39}]\cdot13H_2O$ replaced $K_8Na_2[A-\alpha-GeW_9O_{34}]\cdot25H_2O$ under the similar conditions, they can be not formed, illustrating that the conversion of $[A-\alpha-GeW_9O_{34}]^{10-}$ to $[\alpha-GeW_{11}O_{39}]^-$ is necessary in the formation of them.

Structural descriptions of *1* and *2*

Single-crystal X-ray diffraction indicates that **1** crystallizes in the monoclinic space group $P2_1/c$ and **2** belongs to the triclinic space group $P-1$. The common feature of **1** and **2** is that both consist of 1:2-type $[Ln(\alpha-GeW_{11}O_{39})_2]^{13-}$ subunits with the supporting copper-en cations. The tetrameric molecular unit of **1** is composed of 1 four-supporting tetrameric Keggin-type POM subunit $\{[Cu(en)_2(H_2O)]_2[Cu(en)_2]_2\{Cu(en)_2[Eu(\alpha-GeW_{11}O_{39})_2]_2\}\}^{16-}$, 3 diprotonated $[enH_2]^{2+}$ cations, 2 Na$^+$ cations, 1 K$^+$ cation, 7 proton and 13 lattice water molecules (Fig. 2a). The molecular unit of **1** can be viewed as the fusion of two asymmetric structural units (Fig. S1) by the bridging role of the $[Cu1(en)_2]^{2+}$ cation. Notably, there are three crystallographically unique copper-en cations (namely, $[Cu1(en)_2]^{2+}$, $[Cu2(en)_2(H_2O)]^{2+}$ and $[Cu3(en)_2]^{2+}$) in the molecular unit of **1**. It should be worth noting that the $[Cu1(en)_2]^{2+}$ cation is located on the inversion center $(0,0,1/2)$ of the molecular unit. The $[Cu1(en)_2]^{2+}$ and $[Cu2(en)_2(H_2O)]^{2+}$ cations are embedded in elongated octahedral geometries constituted by four N atoms [Cu–N: 1.95(2)–2.005(15) Å] and two terminal or water O atoms [Cu–O: 2.502(14)–3.190(13) Å] while the $[Cu3(en)_2]^{2+}$ cation is in the square pyramidal geometry formed by four N atoms [Cu–N: 1.92(2)–1.92(2) Å] and a terminal O atom [Cu–O: 2.565(15) Å].

Table 1
Summary of crystallographic data for complexes **1** and **2**.

Data	1	2
Empirical formula	$C_{26}H_{147}Cu_5Eu_2Ge_4KN_{26}Na_2O_{171}W_{44}$	$C_{40}H_{192}Cu_{10}Ge_4La_2N_{40}Na_2O_{170}W_{44}$
Formula weight	12647.16	13293.30
Crystal system	Monoclinic	Triclinic
Space group	$P2_1/c$	$P-1$
a (Å)	17.570(3)	17.607(3)
b (Å)	24.221(4)	18.191(3)
c (Å)	24.700(4)	18.668(3)
α (deg)	90	69.362(3)
β (deg)	104.107(4)	85.639(3)
γ (deg)	90	87.677(4)
V (Å³)	10195(3)	5578.8(17)
Z	2	1
D (g cm⁻³)	4.120	3.957
μ (mm⁻¹)	26.531	24.515
Limiting indices	$-20 \leqslant h \leqslant 20$	$-19 \leqslant h \leqslant 20$
	$-28 \leqslant k \leqslant 25$	$-18 \leqslant k \leqslant 21$
	$-28 \leqslant l \leqslant 29$	$-21 \leqslant l \leqslant 22$
Goodness-of-fit on F^2	1.018	1.030
R_1, wR_2 [$I > 2\sigma(I)$]	0.0464, 0.1145	0.0782, 0.1476
R_1, wR_2 [all data]	0.0801, 0.1313	0.1184, 0.1537
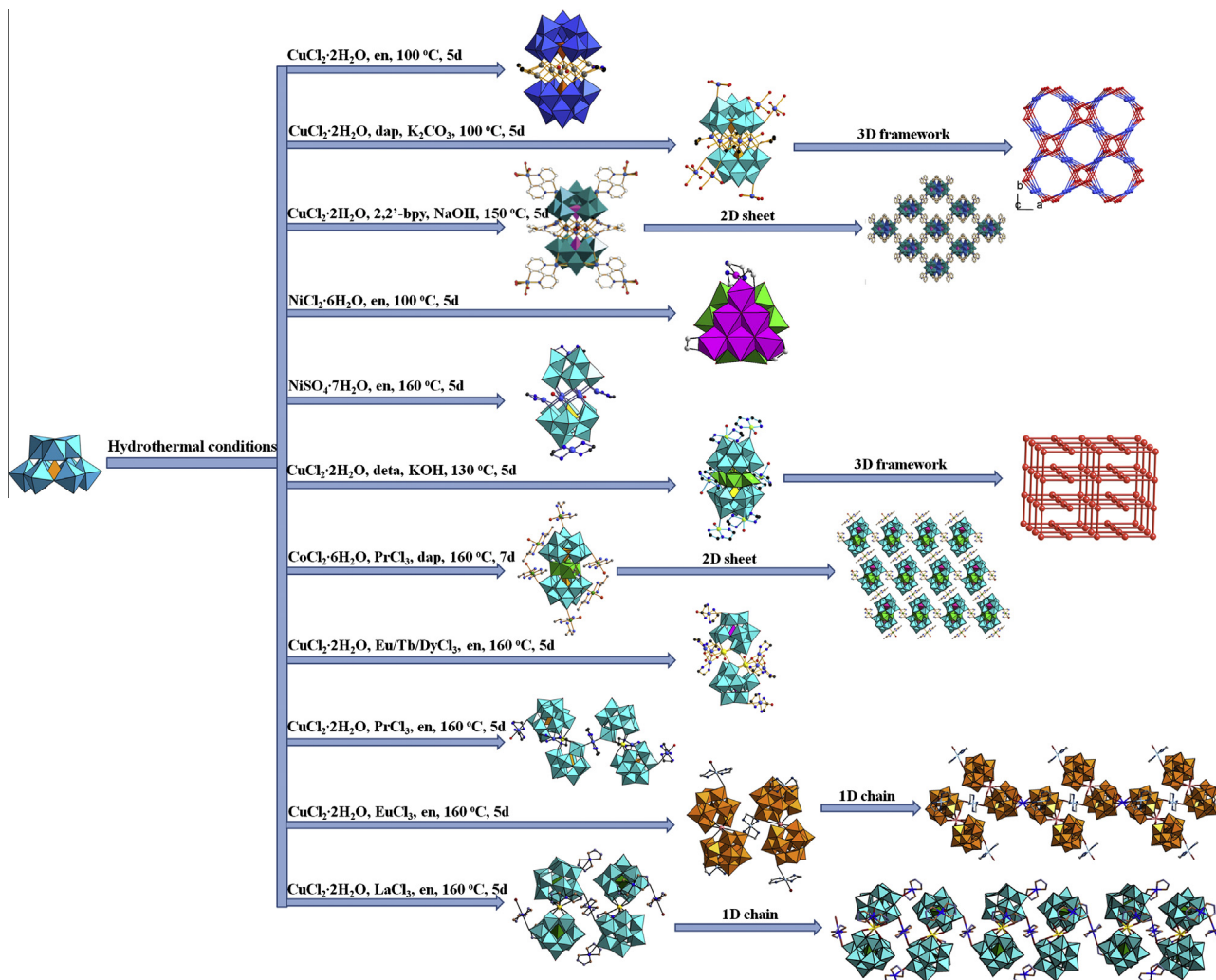
Fig. 1. The summary of the synthetic condition and related phases in the $[A-\alpha-GeW_9O_{34}]^{10-}$ reaction system.

The eight-coordinate Eu1 cation is sandwiched by two monolacunary $[\alpha-GeW_{11}O_{39}]^{8-}$ moieties resulting in a well-known sandwich-type bis(undecatungstogermanate)lanthanate [Eu(α-Ge $W_{11}O_{39})_2]^{13-}$ unit. Such 1:2-type structural type was firstly discovered by Peacock and Weakly in 1971 [33] and this 1:2 structural series made up of one Ln cation and two monovacant Keggin-type POM units have been widely investigated [34,35]. The Eu1 cation shows the distorted square antiprismatic geometry with the Eu–O distances of 2.380(13)–2.470(14) Å (Fig. 2b). In the coordination polyhedron around the Eu1 cation, the O27, O31, O36 and O39 atoms and the O40, O48, O71 and O68 atoms create two bottom surfaces of the square antiprism, and their average deviations from their least-squares surfaces are 0.0067 and 0.0115 Å, respectively. The distances between the Eu1 cation and two bottom surfaces are 1.2437 and 1.2727 Å, respectively. The dihedral angle for two bottom surfaces is 2.60°. The above-mentioned data indicate that the square antiprism is somewhat distorted, which may be related to the distortion of $[Eu(\alpha-GeW_{11}O_{39})_2]^{13-}$ unit resulting from the influence of copper-en cation, $[enH_2]^{2+}$, Na$^+$ and K$^+$ cations in its periphery. It is worth noting that that adjacent four-supporting tetrameric units in **1** are combined with each other via eight-coordinate K1 cations (Fig. 2c), giving rise to a 1D chain architecture (Fig. 2d), in where the K1 cation displays the severely distorted square prismatic geometry with the K–O distances of 2.807(13)–

2.836(14) Å. The 1D chain fashion in **1** is the same to that observed in KNa$_2$H$_7$[enH$_2$]$_3$[Cu(en)$_2$(H$_2$O)]$_2$[Cu(en)$_2$]$_2${Cu(en)$_2$[Er(α-Ge W$_{11}$O$_{39}$)$_2$]$_2$}·15H$_2$O reported by us recently [26].

Different from **1**, the asymmetric structural unit of **2** is composed of one 1:2-type $[La(\alpha-GeW_{11}O_{39})_2]^{13-}$ core, four $[Cu(en)_2]^{2+}$ cations, one free $[Cu(en)_2(H_2O)]^{2+}$ cation, one Na$^+$ ion, two protons and six lattice water molecules (Fig. 3a). There are six crystallographically independent copper-en cations (namely, $[Cu1(en)_2]^{2+}$, $[Cu2(en)_2]^{2+}$, $[Cu3(en)_2]^{2+}$, $[Cu4(en)_2]^{2+}$, $[Cu5(en)_2(H_2O)]^{2+}$ and $[Cu6(en)_2]^{2+}$), in which the $[Cu2(en)_2]^{2+}$ and $[Cu4(en)_2]^{2+}$ cations are situated on the special positions with the site occupancy factor of 0.5 while the remaining copper-en cations occupy the usual sites with the site occupancy factor of 1 for each. The $[Cu1(en)_2]^{2+}$, $[Cu3(en)_2]^{2+}$ and $[Cu6(en)_2]^{2+}$ cations act as the supporting groups linking to the $[La(\alpha-GeW_{11}O_{39})_2]^{13-}$ core whereas the $[Cu2(en)_2]^{2+}$ and $[Cu4(en)_2]^{2+}$ cations function as the bridging cations connecting neighboring the $[La(\alpha-GeW_{11}O_{39})_2]^{13-}$ cores. The $[Cu1(en)_2]^{2+}$, $[Cu3(en)_2]^{2+}$, $[Cu5(en)_2(H_2O)]^{2+}$ and $[Cu6(en)_2]^{2+}$ cations show the square pyramid geometries defined by four N atoms from two en ligands [Cu–N: 1.86(4)–2.08(3) Å] and one terminal or water O atom [Cu–O: 2.395 (18)–2.850(21) Å]. The $[Cu2(en)_2]^{2+}$ and $[Cu4(en)_2]^{2+}$ cations display the octahedral geometry built by four N atoms from two en ligands [Cu–N: 1.93(4)–2.04(2) Å] and two terminal O atoms from adjacent two 1:2-type [La(α-PW$_{11-}$
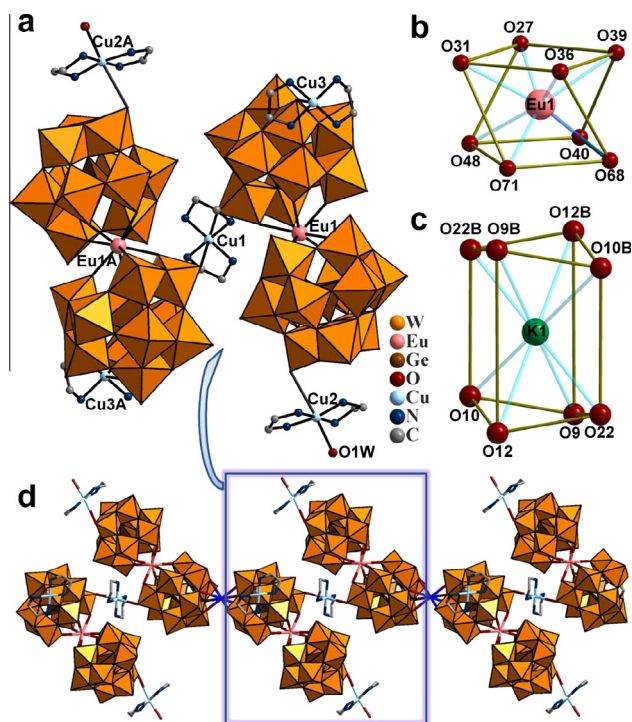
Fig. 2. (a) The tetrameric molecular unit of **1** with selected numbering scheme. Hydrogen atoms, Na$^+$, K$^+$ cations and lattice water molecules are omitted for clarity. (b) The distorted square antiprismatic coordination geometry around the Eu1 cation. (c) The distorted square prismatic coordination geometry around the K1 cation. (d) The 1D chain architecture formed by $\{[Cu(en)_2(H_2O)]_2[Cu(en)_2]_2\{Cu(en)_2[Eu(\alpha\text{-}GeW_{11}O_{39})_2]_2\}\}^{16-}$ units through K$^+$ cations. The atoms with the suffix codes A and B are generated by the symmetry operation. A: $-x, -y, 1-z$; B: $-x, 1-y, 1-z$.

$O_{39})_2]^{11-}$ subunits [Cu–O: 2.847(23)–2.995(23) Å]. The La1 cation also inhibits in the distorted square antiprismatic geometry with La–O distances of 2.460(18)–2.604(16) Å (Fig. S2). Analogous to **1**, two asymmetric structural units of **2** can be combined together by means of the [Cu2(en)$_2$]$^{2+}$ cation forming the tetrameric molecular unit $[[Cu(en)_2]_6[Cu(en)_2]\{Cu(en)_2[La(\alpha\text{-}GeW_{11}O_{39})_2]_2\}]^{10-}$ (Fig. 3b). The most remarkable charateric of **2** is that tetrameric molecular units are interconnected via [Cu4(en)$_2$]$^{2+}$ bridges giving rise to a 1D extended chain (Fig. 3c). From the above discussion we can see three main differences between **1** and **2**: (a) there are three crystallographically unique copper-en cations in **1** while six crystallographically unique copper-en cations exist in **2**; (b) the tetrameric molecular unit of **1** is four-supporting whereas the tetrameric molecular unit of **2** is six-supporting; (c) the 1D chain in **1** is constructed from the tetrameric molecular units by the square antiprismatic K$^+$ connectors, in contrast, the 1D chain in **2** is established by the tetrameric molecular units through the octahedral [Cu(en)$_2$]$^{2+}$ linkages.

IR spectra

IR spectra of **1–2** have been recorded between 4000 and 400 cm^{-1} with KBr pellets (Fig. 4). In the low-wavenumber region ($\nu < 1000$ cm^{-1}), Both exhibit the characteristic ν(Ge–O$_a$), terminal ν(W–O$_t$), corner-sharing ν(W–O$_b$) and edge-sharing ν(W–O$_c$) asymmetrical vibration patterns derived from Keggin-type GT frameworks, which are observed at 878; 939; 817, 757; and 706 cm^{-1} for **1**, 872; 938; 813, 757; and 707 cm^{-1} for **2**, respectively. Compared to K$_6$Na$_2$[(α-GeW$_{11}$O$_{39}$)]·13H$_2$O prepared according to the reference [36], the ν(W–O$_t$) vibration band for **1** and **2** is almost not shifted, suggesting that [Cu(en)$_2$(H$_2$O)]$^{2+}$ and
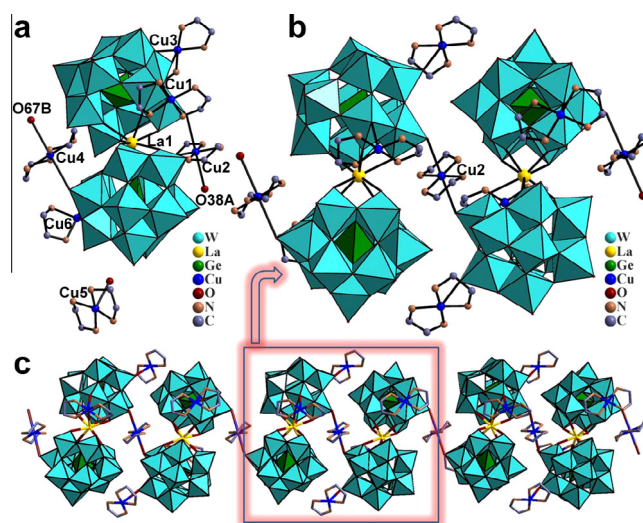
Fig. 3. (a) The asymmetrical molecular unit of **2** with selected numbering scheme. Hydrogen atoms, Na$^+$ cations and lattice water molecules are omitted for clarity. (b) The tetrameric molecular unit of **2** with selected numbering scheme. (c) The 1D extended chain constructed from tetrameric molecular units via [Cu4(en)$_2$]$^{2+}$ bridges. The atoms with the suffix codes A and B are generated by the symmetry operation. A: $2-x, -y, 1-z$; B: $1-x, -y, 2-z$.

[Cu(en)$_2$]$^{2+}$ cations have a weak influence on the terminal oxygen atoms on the [α-GeW$_{11}$O$_{39}$]$^{8-}$ fragments, which well coincides with the longer Cu–O distances (>2.35 Å) from the X-ray single-crystal analysis. Furthermore, the resonances at 3308–3146 cm^{-1} and 2952–2892 cm^{-1} are assigned to the ν(NH$_2$) and ν(CH$_2$) stretching vibration, and the signals at 1589–1583 cm^{-1} and 1474–1463 cm^{-1} correspond to the δ(NH$_2$) and δ(CH$_2$) bending vibration, respectively. These resonance signals confirm the existence of en groups. Additionally, the occurrence of the vibration band at 3446–3435 cm^{-1} suggests the presence of lattice water molecules or coordination water molecules. By and large, the results of the IR spectra are good consistence with the single-crystal structural analysis.

The solid-state electrochemical and electrocatalytic properties of 1

It is well known that the ability of POMs undergoing reversible multielectron redox processes makes them very attractive in the chemically-modified electrode and electrocatalytic study [37]. Because **1** is hydrothermally obtained and has poor solubility in
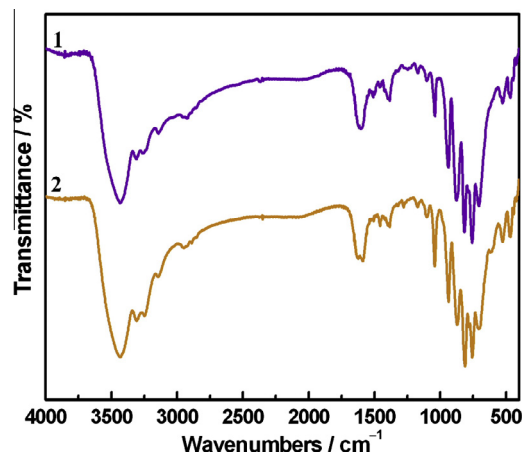
Fig. 4. IR spectra of **1** and **2**.

aqueous solution, **1** can be used as the modified carbon paste electrode (**1**-CPE) to investigate the electrochemical behavior and electrocatalytic activity. The cyclic voltammograms for **1**-CPE in a pH = 0.81 in 0.5 mol L^{-1} Na$_2$SO$_4$ + H$_2$SO$_4$ aqueous solution at different scan rates are presented in Fig. 5. In the potential range of −0.8 V to 0.4 mV, it can be clearly seen that there are two pairs of reversible redox peaks (I–I′ and II–II″) with the mean peak potentials $E_{1/2} = (E_{pc} + E_{pa})/2$ at −0.022 V and −0.574 V (scan rate: 50 mV/s), which can be respectively ascribed to the redox process of the Cu^{II} centers [38] and the redox process of the W^{VI} atoms in [Eu(α-GeW$_{11}$O$_{39}$)$_2$]$^{13-}$ fragments [39]. From Fig. 5 we can see that with the scan rates increasing, the cathodic peak potentials of the W^{VI} wave and the Cu^{II} wave slightly shift to the negative direction and the corresponding anodic peak potentials slightly shift toward the positive direction. The peak-to-peak separation between the corresponding cathodic and anodic peaks slightly increases, but the mean peak potential does not change on the whole. The reason why the peak-to-peak separations between the corresponding anodic and cathodic peaks increase with increasing the scan rate may be related two factors: (a) the reduction of **1** immobilized in the CPE is accompanied by the evolution of protons from solution to maintain charge neutrality [40]; (b) the electron exchange rate between the insoluble solid **1** and the electrode may be slower than that between the soluble POM anions and the electrode [40]. Usually, the scan rate can influence the electrochemical behavior. As a result, the influence of the scan rate on the electrochemical behavior for **1** has been investigated. The results show that the peak current is proportional to the scan rate (Fig. S3), indicating that the redox process of **1**-CPE is surface-controlled when the scan rate is lower than 100 mV s^{-1}, however, the peak current is proportional to the square root of the scan rate (Fig. S4), which suggests that the redox process of **1**-CPE is diffusion-controlled when the scan rate is higher than 100 mV s^{-1} [40]. The influence of the scan rate on the electrochemical behavior observed in **1**-CPE is very similar to those in (Hbpy)$_4$[SiMo$_{12}$O$_{40}$]-CPE and [Cu(bbi)]$_5$H [H$_2$W$_{12}$O$_{40}$]-CPE reported by Peng and coworkers [39,40]. As we know, the reduction of nitrite to ammonia involves a six-electron-eight-proton change [40], the direct electroreduction of nitrite requires a large overpotential at most electrode surfaces, therefore, no obvious response is observed for nitrite at a bare CPE in the potential range of −0.8 to +4 V in 0.5 mol L^{-1} Na$_2$SO$_4$ + H$_2$SO$_4$ aqueous solution [41]. However, Fig. 6 shows the cyclic voltammograms of **1**-CPE at the scan rate of 50 mV s^{-1} in the acid 0.5 mol L^{-1} Na$_2$SO$_4$ + H$_2$SO$_4$ aqueous solution (pH = 0.81) containing sodium nitrite. Obviously, with the addition of sodium nitrite,
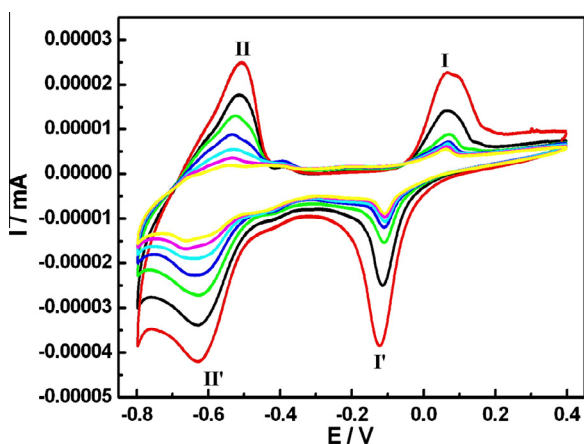
the reduction peak current of the W^{VI}-based wave increases markedly while the corresponding oxidation peak current decreases gradually, which indicates that the reduction of nitrite is mediated by the reduced species of germanotugstate polyoxoanions and **1**-CPE displays good electrocatalytic activity toward the reduction of nitrite.

Photoluminescence properties

Ln-containing compounds have aroused much attention because of their unique luminescent properties and various applications as functional materials in low-energy scintillators, light-emitting diodes, tunable lasers, NIR-emitting materials and sensory probes [42], which involve mainly in the fact that the electronic energy levels of Ln ions are well defined due to the shielding of the 4f orbitals by the filled 5s^{2}5p^6 subshells, and they are less sensitive to the chemical environments around lanthanide ions [43], thus, Ln ions retain their atomic properties upon complex formation. Consequently, each Ln ion exhibits narrow and characteristic 4f–4f transitions. Ln ions suffer from weak light absorption due to the forbidden f–f transitions, making the direct excitation of the metals very inefficient unless high-power laser excitation is utilized. This problem can be overcome by coupling species that can participate in energy transfer processes, known as "luminescence sensitization" [44]. Photoexcitation of the O → M (M = Mo or W) ligand to metal charge transfer (LMCT) bands of the POM lattice can result in intramolecular energy transfer from the O → M excited states to excited energy levels of Ln^{III} ions, thereby sensitizing Ln^{III} emission [45]. The photoluminescence behavior of some POMs containing Ln cations has been investigated by Yamase and other groups [46–50]. Furthermore, the molecular mechanisms of intramolecular energy transfer processes have been also comprehensively probed by Yamase [46]. The emission characteristics of Ln^{III} ions are highly dependent on the nature of POM units, the symmetry and coordination geometry at the Ln centers and the number of aqua coligands. Indeed, POM units bound to Ln^{III} ions are usually polydentate, minimizing the coligation of aqua and similar ligands, which consist of high frequency O–H and N–H oscillators that tend to quench the luminescence emission [45]. As a result, the solid-state photoluminescence property of **1** has been investigated at room temperature. When the as-synthesized solid of **1** was measured under excitation at 392 nm, the characteristic emission bands of the Eu^{III} ions are observed at 558 nm, 573 nm, 593 nm, 612 nm, 645 nm and 706 nm (Fig. 7), which are attributed to $^5D_1 \rightarrow {}^7F_2$, $^5D_0 \rightarrow {}^7F_0$, $^5D_0 \rightarrow {}^7F_1$, $^5D_0 \rightarrow {}^7F_2$, $^5D_0 \rightarrow {}^7F_3$

Fig. 5. The cyclic voltammograms of **1**-CPE in 0.5 mol L^{-1} Na$_2$SO$_4$ + H$_2$SO$_4$ aqueous solution (pH = 0.81) at the different scan rates. From inner to outer: 20, 50, 80, 110, 140, 170, and 200 mV s^{-1}.
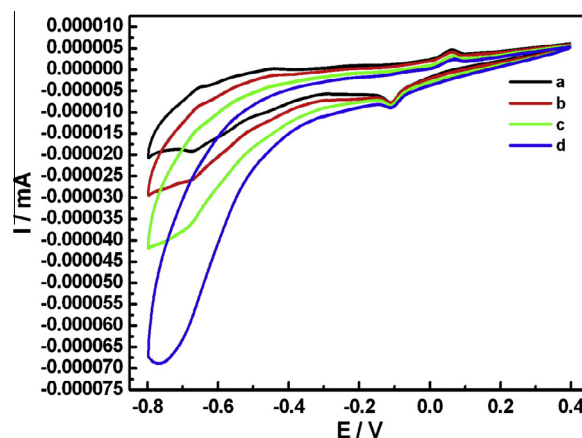
Fig. 6. Cyclic voltammograms of the **1**-CPE in 0.5 mol L^{-1} Na$_2$SO$_4$ + H$_2$SO$_4$ aqueous solution (pH = 0.81, 50 mL) containing 1 × 10^{-3} (a); 3 × 10^{-3} (b); 5 × 10^{-3} (c); 7 × 10^{-3} (d) mol L^{-1} NaNO$_2$. Scan rate: 50 mV s^{-1}.

and $^5D_0 \rightarrow {}^7F_4$ transitions, respectively [51]. The magnetic dipole $^5D_0 \rightarrow {}^7F_{1,3}$ transitions are insensitive to their local environments while the electric dipole $^5D_0 \rightarrow {}^7F_{0,2,4}$ transitions are hypersensitive to their local environments [52]. The $^5D_0 \rightarrow {}^7F_0$ transition is strictly forbidden in a field of symmetry, but this symmetrically forbidden transition at 573 nm can be hardly found in **1**, suggesting that **1** utilizes the comparatively higher symmetry. The $^5D_0 \rightarrow {}^7F_1$ transition at 593 nm is a magnetic-dipole transition and its intensity varies with the crystal field strength acting on Eu^{III} ions. The $^5D_0 \rightarrow {}^7F_2$ transition at 612 nm is an electric dipole transition and is extremely sensitive to the chemical bonds in the vicinity of Eu^{III} ions. Therefore, the intensity ratio of the $^5D_0 \rightarrow {}^7F_2/{}^5D_0 \rightarrow {}^7F_1$ transitions is widely used to check the chemical microenvironment of around the Eu^{III} ion and is acted as a measure of the site symmetry of the Eu^{III} ions [53]. In a site environment with inversion symmetry, the $^5D_0 \rightarrow {}^7F_1$ magnetic dipole transition is dominant while in a site environment without inversion symmetry, the $^5D_0 \rightarrow {}^7F_2$ electronic dipole transition becomes the strongest one [54]. The intensity ratio of the $^5D_0 \rightarrow {}^7F_2/{}^5D_0 \rightarrow {}^7F_1$ transition in **1** is *ca.* 0.15, indicating that the site environment of the Eu^{III} ion in **1** have a higher symmetry, which is in good agreement with the fact that the square-antiprismatic Eu1 ion is sandwiched by eight oxygen atoms from two $[\alpha\text{-}GeW_{11}O_{39}]^{8-}$ subunits. Such luminescent behavior of **1** is somewhat different from those of $\{[Cu(en)_2(H_2O)][Cu_3Eu(en)_3 (OH)_3(H_2O)_2](\alpha\text{-}GeW_{11}O_{39})\}_2 \cdot 11H_2O$ [26] and $[Cu(dap)_2(H_2O)]_2 \{Cu(dap)_2[\alpha\text{-}H_2SiW_{11}O_{39}Eu(H_2O)_3]_2\} \cdot 10H_2O$ [55] previously reported by us, the main reason of which is that their coordination environments of the Eu^{III} ions are different.

Summary

In conclusion, we have hydrothermally prepared and structurally characterized two Cu–Ln heterometallic GT hybrids. **1** exhibits the 1D chain motif built by tetrameric $\{[Cu(en)_2(H_2O)]_2[Cu(en)_2]_2 \{Cu(en)_2[Eu(\alpha\text{-}GeW_{11}O_{39})_2]\}\}^{16-}$ moieties through square antiprismatic K^+ cations while **2** displays the 1D architecture made by tetrameric $[[Cu(en)_2]_6[Cu(en)_2]_2\{Cu(en)_2[La(\alpha\text{-}GeW_{11}O_{39})_2]_2\}]^{10-}$ units via octahedral $[Cu(en)_2]^{2+}$ cations. By comparison of the synthetic conditions **1** and **2** with those Cu–Ln heterometallic GTs previously reported by us [26], a conclusion can be made that the molar ratios of $K_8Na_2[A\text{-}\alpha\text{-}GeW_9O_{34}] \cdot 25H_2O/CuCl_2 \cdot 2H_2O/LnCl_3$ have an important influence on the structural diversity of the resulting GT derivatives. Moreover, **1** is used to make the modified electrode to electrocatalyze the reduction of nitrite and the results indicate that the **1**-CPE has a good electrocatalytic activity toward the reduction of nitrite. The solid-state photoluminescence property of **1** has been investigated at room temperature. Photoexcitation of the as-synthesized solid of **1** at 392 nm displays six characteristic emission bands of the Eu^{III} ions. In the following work, the N/O-containing functional ligands, variable TM cations and POM precursors will be introduced to our research system to obtain much more TM–Ln heterometallic GTs with unexpected structures and properties.

Acknowledgments

Appendix A. Supplementary material

Crystallographic data have been deposited with the Cambridge Crystallographic Data Center as supplementary publication CCDC 920432 for **1** and CCDC 920433 for **2**. Copies of the data can be obtained free of charge on application to CCDC, 12 Union Road, Cambridge CB2 1EZ, UK (Fax: +44 1223 336 033, e-mail: deposit@ccdc.cam.ac.uk). Supplementary data associated with this article can be found, in the online version, at http://dx.doi.org/10.1016/j.saa.2013.05.054.

References

[1] S. Reinoso, M. Giménez-Marqués, J.R. Galán-Mascarós, P. Vitoria, J.M. Gutiérrez-Zorrilla, Angew. Chem. Int. Ed. 49 (2010) 8384–8388.
[2] A.H. Ismail, B.S. Bassil, G.H. Yassin, B. Keita, U. Kortz, Chem. Eur. J. 18 (2012) 6163–6166.
[3] S. Reinoso, Dalton Trans. 40 (2011) 6610–6615.
[4] Z.M. Zhang, Y.G. Li, S. Yao, E.B. Wang, Dalton Trans. 40 (2011) 6475–6479.
[5] D.Y. Shi, S.S. Shang, L.J. Chen, X.M. Cai, X. Wang, J.W. Zhao, Syn. Met. 162 (2012) 1030–1036.
[6] X.J. Feng, W.Z. Zhou, Y.G. Li, H.S. Ke, J.K. Tang, R. Clérac, Y.H. Wang, Z.M. Su, E.B. Wang, Inorg. Chem. 51 (2012) 2722–2724.
[7] J.D. Compain, K. Nakabayashi, S. Ohkoshi, Inorg. Chem. 51 (2012) 4897–4899.
[8] Z.M. Zhang, E.B. Wang, W.L. Chen, H.Q. Tan, Aust. J. Chem. 60 (2007) 284–290.
[9] N.H. Nsouli, A.H. Ismail, I.S. Helgadottir, M.H. Dickman, J.M. Clemente-Juan, U. Kortz, Inorg. Chem. 48 (2009) 5884–5890.
[10] L. Chen, L. Li, B. Liu, G. Xue, H. Hu, F. Fu, J. Wang, Inorg. Chem. Commun. 12 (2009) 1035–1037.
[11] U. Kortz, S. Nellutla, A.C. Stowe, N.S. Dalal, U. Rauwald, W. Danquah, D. Ravot, Inorg. Chem. 43 (2004) 2308–2317.
[12] T. Yamase, H. Abe, E. Ishikawa, H. Nojiri, Y. Ohshima, Inorg. Chem. 48 (2009) 138–148.
[13] L.H. Bi, U. Kortz, S. Nellutla, A.C. Stowe, J. van Tol, N.S. Dalal, B. Keita, L. Nadjo, Inorg. Chem. 44 (2005) 896–903.
[14] N.H. Nsouli, S.S. Mal, M.H. Dickman, U. Kortz, B. Keita, L. Nadjo, J.M. Clemente-Juan, Inorg. Chem. 46 (2007) 8763–8770.
[15] N. Jiang, F. Li, L. Xu, Y. Li, J. Li, Inorg. Chem. Commun. 13 (2010) 372–375.
[16] J.W. Zhao, J. Zhang, S.T. Zheng, G.Y. Yang, Chem. Commun. (2008) 570–572.
[17] J.W. Zhao, S.T. Zheng, Z.H. Li, G.Y. Yang, Dalton Trans. (2009) 1300–1306.
[18] Y.G. Li, L. Xu, G.G. Gao, N. Jiang, H. Liu, F.Y. Li, Y.Y. Yang, CrystEngComm 11 (2009) 1512–1514.
[19] B.S. Bassil, M.H. Dickman, I. Romer, B. vonder Kammer, U. Kortz, Angew. Chem. Int. Ed. 46 (2007) 6192–6195.
[20] J.P. Wang, J.W. Zhao, X.Y. Duan, J.Y. Niu, Cryst. Growth Des. 6 (2006) 507–513.
[21] J.P. Wang, X.Y. Duan, X.D. Du, J.Y. Niu, Cryst. Growth Des. 6 (2006) 2266–2270.
[22] S. Reinoso, J.R. Galán-Mascarós, Inorg. Chem. 49 (2010) 377–379.
[23] S. Reinoso, J.R. Galán-Mascarós, L. Lezama, Inorg. Chem. 50 (2011) 9587–9593.
[24] W.D. Wang, X.X. Li, W.H. Fang, G.Y. Yang, J. Clust. Sci. 22 (2011) 87–95.
[25] B. Li, J.W. Zhao, S.T. Zheng, G.Y. Yang, Inorg. Chem. 48 (2009) 8294–8303.
[26] J.W. Zhao, D.Y. Shi, L.J. Chen, Y.Y. Li, P.T. Ma, J.P. Wang, J.Y. Niu, Dalton Trans. 41 (2012) 10740–10751.
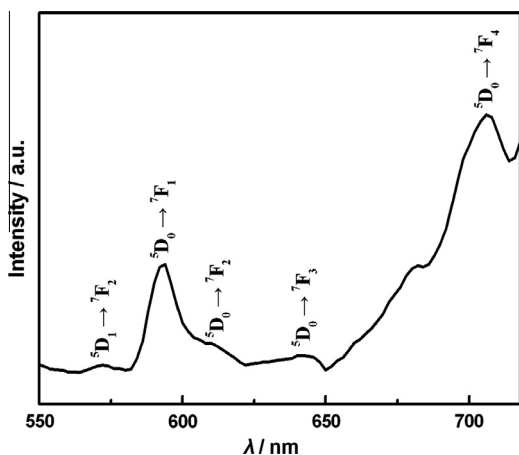
Fig. 7. The solid-state emission spectrum for **1** at room temperature. The emission spectrum was recorded at λ_{ex} = 392 nm.

[27] G.M. Sheldrick, SHELXS-97, Program for Crystal Structure Solution, Springer, Berlin, 1997.

[28] G.M. Sheldrick, SHELXL-97, Program for Crystal Structure Refinement, Springer, Berlin, 1997.

[29] J.W. Zhao, C.M. Wang, J. Zhang, S.T. Zheng, G.Y. Yang, Chem. Eur. J. 14 (2008) 9223–9239.

[30] J.W. Zhao, J. Zhang, Y. Song, S.T. Zheng, G.Y. Yang, Eur. J. Inorg. Chem. (2008) 3809–3819.

[31] W.J. Niu, D.Y. Shi, J.W. Zhao, X.M. Cai, L.J. Chen, Inorg. Chem. Commun. 17 (2012) 79–83.

[32] L.J. Chen, D.Y. Shi, J.W. Zhao, Y.L. Wang, P.T. Ma, J.Y. Niu, Inorg. Chem. Commun. 14 (2011) 1052–1056.

[33] R.D. Peacock, T.J.R. Weakley, J. Chem. Soc. A (1971) 1836–1839.

[34] P. Mialane, L. Lisnard, A. Mallard, J. Marrot, E. Antic-Fidancev, P. Aschehoug, D. Vivien, F. Sécheresse, Inorg. Chem. 42 (2003) 2102–2108.

[35] D.Y. Shi, J.W. Zhao, L.J. Chen, P.T. Ma, J.P. Wang, J.Y. Niu, CrystEngComm 14 (2012) 3108–3119.

[36] J.W. Zhao, D.Y. Shi, L.J. Chen, P.T. Ma, J.P. Wang, J.Y. Niu, CrystEngComm 13 (2011) 3462–3469.

[37] Z.G. Han, Y.L. Zhao, J. Peng, Y.H. Feng, J.N. Yin, Q. Liu, Electroanalysis 17 (2005) 1097–1102.

[38] A. Salimi, A. Korani, R. Hallaj, R. Khoshnavazi, H. Hadadzadeh, Anal. Chim. Acta 635 (2009) 63–70.

[39] P.P. Zhang, J. Peng, X.Q. Shen, Z.G. Han, A.X. Tian, H.J. Pang, J.Q. Sha, Y. Chen, M. Zhu, J. Solid State Chem. 182 (2009) 3399–3405.

[40] Z.G. Han, Y.L. Zhao, J. Peng, Q. Liu, E.B. Wang, Electrochim. Acta 51 (2005) 218–224.

[41] B. Keita, L. Nadjo, J. Electroanal. Chem. Interfacial Electrochem. 227 (1987) 77–98.

[42] J.C.G. Bünzli, C. Piguet, Chem. Soc. Rev. 34 (2005) 1048–1077.

[43] G.J. Sopasis, M. Orfanoudaki, P. Zarmpas, A. Philippidis, M. Siczek, T. Lis, J.R. O'Brien, C.J. Milios, Inorg. Chem. 51 (2012) 1170–1179.

[44] Y. Cui, Y. Yue, G. Qian, B. Chen, Chem. Rev. 112 (2012) 1126–1162.

[45] C. Ritchie, V. Baslon, E.G. Moore, C. Reber, C. Boskovic, Inorg. Chem. 51 (2012) 1142–1151.

[46] T. Yamase, Chem. Rev. 98 (1998) 307–325.

[47] T. Yamase, T. Kobayashi, M. Sugeta, H. Naruke, J. Phys. Chem. A 101 (1997) 5046–5053.

[48] T. Yamase, H. Naruke, J. Chem. Soc., Dalton Trans. (1991) 285–292.

[49] I. Creaser, M.C. Heckel, R.J. Neitz, M.T. Pope, Inorg. Chem. 32 (1993) 1573–1578.

[50] X. Wang, Y. Guo, Y. Li, E. Wang, C. Hu, N. Hu, Inorg. Chem. 42 (2003) 4135–4140.

[51] J. Xia, B. Zhao, H.S. Wang, W. Shi, Y. Ma, H.B. Song, P. Cheng, D.Z. Liao, S.P. Yan, Inorg. Chem. 46 (2007) 3450–3458.

[52] Q.H. Xu, L.S. Li, X.S. Liu, R.R. Xu, Chem. Mater. 14 (2002) 549–555.

[53] T. Zhang, C. Spitz, M. Antonietti, C.F.J. Faul, Chem. Eur. J. 11 (2005) 1001–1009.

[54] Y. Su, L. Li, G. Li, Chem. Mater. 20 (2008) 6060–6063.

[55] J.W. Zhao, J. Luo, L.J. Chen, J. Yuan, H.Y. Li, P.T. Ma, J.P. Wang, J.Y. Niu, CrystEngComm 14 (2012) 7981–7993.